PCCP

Accepted Manuscript

ROYAL SOCIETY OF CHEMISTRY

www.rsc.org/pccp

Physical Chemistry Chemical Physics
CREATED USING THE RSC LaTeX PCCP ARTICLE TEMPLATE – SEE www.rsc.org/electronicfiles FOR DETAILS
ARTICLE TYPE
www. rsc.org/xxxxxx | XXXXXXXX

Extraordinary Deformation Capacity of Smallest Carbohelicene Springs

Petr Šesták,[ab†] Jianyang Wu,[bc] Jianying He,[b] Jaroslav Pokluda[ad] and Zhiliang Zhang,*[b]

Received Xth XXXXXXXXXX 20XX, Accepted Xth XXXXXXXXX 20XX
First published on the web Xth XXXXXXXXXX 200X
DOI: 10.1039/b000000x

The extraordinary deformation and loading capacity of nine different [∞]carbohelicene springs under uniaxial tension up to their fracture were computed using the density functional theory. The simulations comprised either the experimentally synthetized springs of hexagonal rings or the hypothetical ones that contained irregularities (defects) as, for example, pentagons replacing the hexagons. The results revealed that the presence of such defects can significantly improve mechanical properties. The maximum reversible strain varied from 78 % to 222 %, the maximum tensile force varied in the range of 5 nN to 7 nN and, moreover, the replacement of hexagonal rings by pentagons or heptagons significantly changed the location of double bonds in the helicenes. The fracture analysis revealed two different fracture mechanisms that could be related to configurations of double and single bonds located at the internal atomic chain. Simulations performed with and without van der Waal's interactions between intramolecular atoms showed that these interactions played an important role only in the first deformation stage.

1 Introduction

Helicenes are three-dimensionally helicoidal molecules formed by ortho-fused benzene rings[1]. Excessively intra- and intermolecular π-electron interactions in the polyaromatic system are the consequence of their special structure[2,3]. Benefitting from their helically molecular topology and intrinsically molecular distortion, they possess a series of intriguing chiral, physical, chemical, electronic and optical properties[4–8]. Unlike common polymers, this π-conjugated material has a high aspect ratio, shape persistence, elasticity, etc. As a result of these unique properties, carbohelicenes and their derivatives hold great potential for a variety of applications in domains such as molecular devices, asymmetric catalysis, molecular recognition and self-assemblies, and materials science[9–11].

Carbohelicenes and their derivatives, serving in molecular devices as molecular springs, molecular actuators, molecular ratchet or molecular switches received increasing attention in the past years in chemistry, biology and nanosciences[10–16]. Although their mechanical properties play an important role in these applications, only very rare attempts have been made to evaluate these properties hitherto. Rempala and King[14] reported that polymeric polyelectrolyte helicenes interacted with amio or ionized phosphate groups are able to exhibit maximum relative elongation of 176 ± 4 % or 184 ± 4 % by molecular dynamics calculations with non-debonded force-fields. Using calculations based on the Density Functional Theory (DFT), Rulíšek et al.[5] showed that the elasticity of hydrogen-free carbohelicenes decreased linearly with increas-

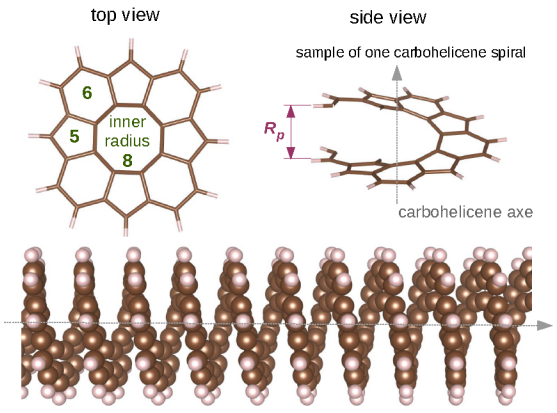

Fig. 1 The spiral structure of carbohelicene N8(5,6) that is constructed by alternating two types of graphene rings (5,6). The length R_p means the spiral (interpitch) distance as well as the length of the simulation box along the carbohelicene axes in the DFT-D2 calculations.

[a] *Faculty of Mechanical Engineering, Brno University of Technology, Technická 2896/2, 616 69 Brno, Czech Republic*
[b] *Faculty of Engineering Science and Technology, Norwegian University of Science and Technology, Rich. Birkelandsvei 1A , 7491 Trondheim, Norway; E-mail: zhiliang.zhang@ntnu.no*
[c] *Research Institute for Biomimetics and Soft Matter, Department of Physics, Xiamen University, 361005 Xiamen, China*
[d] *Central European Institute of Technology, Brno University of Technology, Technická 3058/10, 616 69 Brno, Czech Republic*
† *The results were obtained during author research stay at the NTNU.*

ing number of aromatic rings and the value of the harmonic force constant of carbohelicenes with 14-hexagonal rings was of 99 kJ mol^{-2} Å^{-2}. According to the Hartree-Fock calculations by Jalaie et al.[17], the stiffness of carbohelicenes molecular springs can be modulated by varying the length of the helicene and the electron density and the spring constants of springs with number of coils of 2, 3 and 4 are around 124, 103 and 104 kJ mol^{-2} Å^{-2}, respectively. They argued that the unequal values of constants come from the effects of edge or end of the spring.

Although these pioneering works reported some mechanical parameters of few carbohelicene-based springs, detailed physical insights into molecular deformation mechanisms have not yet been provided. Furthermore, the mechanical responses of carbohelical molecular springs embedded in pentagonal or heptagon defects are not yet studied. In this first principles study we present a mechanical response of nine different carbohelical molecular springs and provide a physical insight into their mechanical stability, deformability and fracture processes at the nanoscale. Such an insight is important for the future use and design of carbohelical molecular springs in the nanoscale molecular devices.

2 Studied structures

All structures presented in this study are [∞]carbohelicenes which means that their lengths along the helical axis are infinite and differ from each other by the a spiral construction where two-dimensional pentagonal, heptagonal and octagonal rings replace some of the hexagonal ones in the original, experimentally observed perfect carbohelicene. This offers many possible structure variations and, therefore, one has to introduce an appropriate nomenclature of individual configurations. Each carbohelicene has been marked as NX(Y,Z) where X means the number of atoms along the internal atomic chain per helicene spiral (see Fig. 1) and Y and Z refer to the kind of carbon rings that were used for its construction. The two numbers in the brackets separated by comma show that the carbohelicene spiral was constructed by alternation of two different rings (e.g. by alternating pentagon and hexagon rings). Some carbohelicene spirals were also predeformed in the equilibrium state to a conical or stairs like shape which was denoted "c" (conical) or "s" (stairs). For example, N8s(5,7) means that the number of atoms along internal chain has an octagonal motif from the top view, "s" represents a stair-like shape of the spiral structure and (5,7) shows that the carbohelicene spiral was constructed from an alternation of pentagon and heptagon carbon rings. If there is only one number in the bracket then only one type of the carbon ring was used for the spiral construction. For example, the perfect carbohelicene is denoted N6(6). The outside bonds of graphene carbohelicenes are terminated by hydrogen atoms.

3 Computational details

In the DFT simulations we utilized the VASP code (Vienna Ab initio Simulation Package)[18–20] together with the PAW pseudopotentials[21] that represents an efficient way how to describe valence electrons. The exchange-correlation energy was evaluated by means of the GGA (Generalized Gradient Approximation) with parametrization of Perdew-Burke-Ernzerhof[22]. The cut off energy was set to 650 eV and the DFT solution was considered to be self-consistent when the total energy difference between two consequent steps was lower than 10^{-06} eV. Meshes containing $3\times3\times17$ k-points were used for integration over the Brillouin zone. We must point out, that during all tensile tests the number of the k-points along the carbohelicene axis was gradually reduced with respect to the carbohelicene elongation to keep equidistant spacing of the k-points in the reciprocal space (eg. 3x3x17 for non-strained helicene to 3x3x5 for strain 222 %). To check if the decreasing of k-points during straining is not creating some irregularities in the dependence $F(\varepsilon)$ we performed an additional tensile test for carbohelicene N8c(5) with constant k-point grid 3x3x17 for entire deformation. The computed results show identical dependences from both approaches. This proves that the decreasing of k-points used in our simulation does not influence the outcomes at all. The structural optimization of the ionic positions was carried out until the forces between each atom were lower than 10^{-2} eV/Å. The method of Grimme DFT-D2[23] that is implemented in the VASP code was used to describe the van der Waal's interactions between intramolecular atoms.

4 Simulation cells and procedures

The simulation cell was represented by the box with lengths of $21\times21\times R_p$ in Å units where R_p is the spiral distance (also called spring pitch) for each individual carbohelicene. The carbohelicene is located in the center of the box and its cylindrical surface is surrounded by vacuum to prevent any interactions which can be caused by the periodic boundary conditions (PBC) in the DFT calculations. The third dimension of the box is parallel to the carbohelicene axis and must be of the same length as the interpitch distance R_p of the simulated carbohelicene. The PBC for this direction reflects an infinite length of simulated springs. In the beginning of the DFT tensile tests, all positions of the atoms were fully optimized to reach the ground-state configuration of minimum energy (free stress state). After that, the uniaxial tensile deformation was applied by gradual stretching of the simulation box in the direction parallel with the carbohelicenes axis. The entire deformation path consisted of incremental deformation steps of 0.25 Å. During each step, the increasing distance R_p^s (strained interpitch distance) produced a homogenous deformation of the spring since the ionic positions in the basis were

Table 1 The summarization of computed results divided into three groups according the the carbohelicene deformation (normal, conical and stair-like) where each group is sorted with respect to the equilibrium total energy per atom E_{tot}^{eq}/N. Other displayed data are related to the structure parameter N (number of atoms in the simulation cell), the non-strained interpitch distance $R_{p,0}$, the maximal value of reversible strain ε_M, the maximal value of the force F_M corresponding to ε_M and the cohesive energy per simulation cell E_c. The last column shows the bonding configuration across internal atomic chain (the most strained atomic chain in the helicenes). For example, C=C penta, C-C hepta means that alternating of double and single bonding can be found at the internal helicene chain and the double boding is located at pentagons while the simple one at heptagons.

	N C/H	$R_{p,0}$ (Å)	ε_M (%)	E_{tot}^{eq}/N (eV)	F_M (nN)	ΔE_c (eV)	bonding at internal chain
N8(5,6)	28/12	3.32	207	-7.41	5.03	12.92	C-C penta, C=C hexa
N6(6)	24/12	3.38	148	-7.28	7.00	13.40	C-C, only hexagons
N6(5,7)	24/12	3.28	176	-7.20	6.74	13.49	C=C penta, C-C hepta
N5(6)	20/10	3.38	096	-7.19	6.62	7.61	C-C only hexagons
N8c(5)	24/08	3.68	222	-7.49	6.20	12.90	C-C=C, only pentagons
N6c(5,6)	21/09	3.50	150	-7.30	6.21	10.69	C-C penta, C=C hexa
N7s(6)	28/14	3.42	124	-7.24	5.38	9.06	C-C, only hexagons
N8s(6)	32/16	4.08	078	-7.18	4.33	5.54	C-C only hexagons
N8s(5,7)	32/16	3.71	155	-7.15	5.49	11.03	C=C penta, C-C hepta

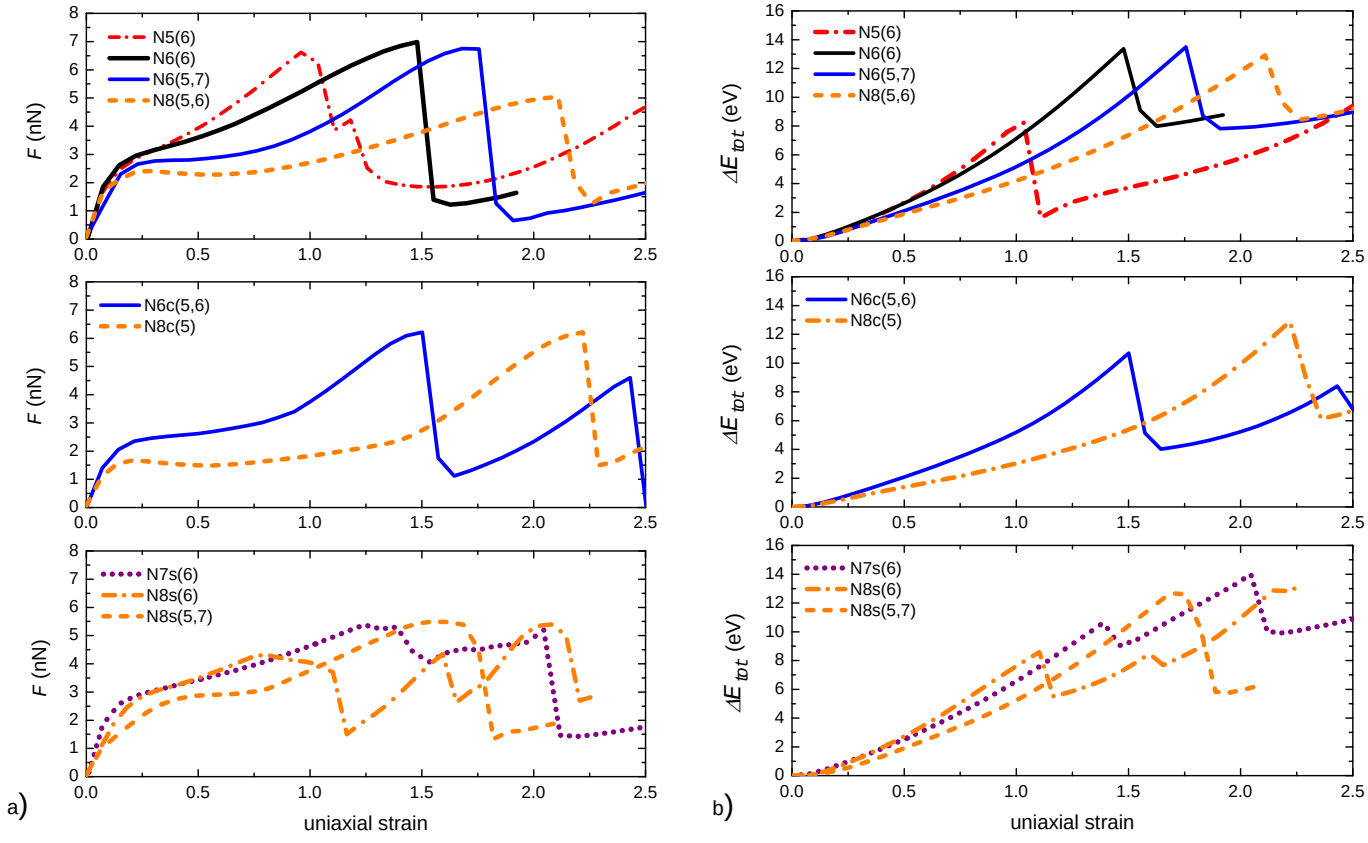

Fig. 2 The force F (the Fig. 2a) and the total energy change per simulation cell ΔE_{tot} (the Fig. 2b) as a function of carbohelicenes elongation in terms of strain ε. The computed results are collected into three groups according to the carbohelicene deformations. The carbohelicene with the same internal atomic chain Nx (pentagonal, hexagonal, heptagonal and octagonal motif from top view) are marked by the same color except the natural one N6(6) which is marked by the black line. The line type like solid or dashed lines are used to make the dependences more distinguishable and they have no special meaning.

set in terms of fractional coordinates. Note that all the ionic positions must have been optimized after each step so the deformation repetitively started from a new ionic configuration.

5 Results

5.1 Mechanical behavior

The mechanical behavior of the carbohelicenes can be described by the dependences of the computed force F (Fig. 2a) and the total energy changes ΔE_{tot} (Fig. 2b) on the applied strain ε where the $\varepsilon = (R_p/R_{p,0} - 1)$. These dependences reflect many characteristics like the elastic/inelastic material response, the loading and deformation capacity, the differences between individual nanosprings and the energy accumulated in the structures during their elongation. Fig. 2a shows that the dependence $F(\varepsilon)$ is of a serrated shape. A similar shape was also obtained for the strain dependence of the total energy change $\Delta E_{tot}(\varepsilon)$ as typical for all types of carbohelicenes. The detailed examination of the atomic configurations during the individual deformation steps revealed that every rapid drop of the load after each local maxima in the $F(\varepsilon)$ dependence corresponded to one broken bond between two carbon atoms. Therefore, the first peak means the first local fracture within the structure, the second peak the second local fracture, etc. Since the heights of the peaks decrease with increasing elongation of the carbohelicenes, the first peak corresponds to the maximal load bearable by the structure. It should be emphasized that, after reaching the first peak, the deformation becomes irreversible due to the related decrease in the total energy E_{tot}. Consequently, the first peak also defines the maximal (ultimate) reversible strain ε_M, i.e., the deformation capacity.

The values of ε_M in Tab. 1 indicate that some types of carbohelicenes can achieve an extraordinary deformation without any irreversible damage due to broken interatomic bonds. This is similar to the deformation behavior of carbon nanotube (CNT) nanosprings[24,25]. The maximal reversible strain ε_M = 222 % belongs to the carbohelicene N8c(5) while the lowest one of 78 % to the carbohelicene N8s(6). It is interesting that these two carbohelicenes are of very similar structures which differ only by their shapes: the N8c(5) spring is of a conical shape while the N8s(6)spring exhibits a stair-like shape which seems to be detrimental for the deformation capacity (see Tab. 1). Indeed, none of stair-shape carbohelicenes reached ε_M higher than 160 % while the values of ε_M for those of conical and standard shapes lie within the range starting from 150 % to 222 %. Thus, the stair-like shape obviously has a negative influence on the deformation capacity of carbohelicenes by reducing their maximal reversible strain. The only exception to the rule is the N5(6) spring that, however, has a small number of atoms at internal chain that any high values of ε_M cannot be expected. The strain capacity of the "natural" carbohelicene N6(6) is the lowest one among the conical and standard springs but, on the other hand, it has the highest loading capacity F_M.

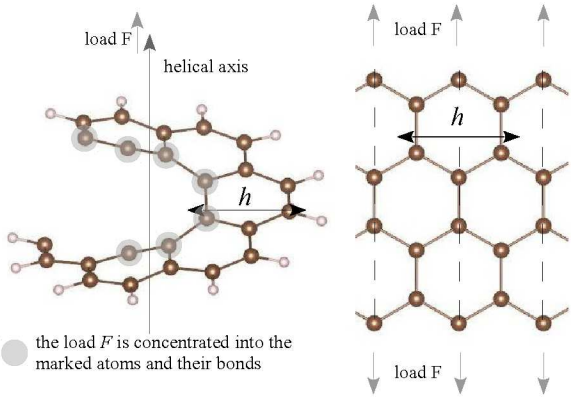

Fig. 3 The sample of the cabohelicene N6(6) with marked spiral of the width h on the left along with the perfect structure of the graphene on the right. Maximal loaded atoms in the carbohelicene spiral during the tensile test are marked by gray circles. The distance h in the graphene corresponds to the widh of the carbohelicene spiral. This width is somewhat greater than that of the hexagon since some enjambment of the covalent electrons should be considered.

The atomic bonds in the deformed carbohelicenes are subjected to a rather complex mixture of tensile, bending and torsion loading. According to a detailed analysis of distances between individual carbon atoms before and after the critical deformation, the tensile stresses is dominant in the final deformation stages. For this reason, one can perform a very approximate comparison of tensile strengths of the perfect carbohelicene N6(6) and graphene. The analysis also revealed that the bonds between the inner atoms of the spiral were subjected to a maximum loading while the outer ones remained practically unstrained. Therefore, only a half-width $h/2$ of the N6(6)spiral was used to recalculate the maximum applied force $F_M = 7.0$ nN into the effective tensile strength stress $\sigma_{eff,u}$ according to the following simple formula $\sigma_{eff,u} = 2F_M/bh$. Here $b = 3.34$ Å is the graphite interplanar distance and $h = 3.47$ Å is the width of the spiral (see Fig. 3). The effective tensile strength $\sigma_{eff,u} = 117$ GPa, calculated in this way, is well comparable to the tensile strength $\sigma_{u,t} = 110$ - 121 GPa of a perfect graphene computed using ab initio methods[26] as well as with $\sigma_{u,exp} = 130 \pm 10$ GPa measured by nanoindenation[27].

A bilinear-like stress-strain response at the onset of deformation was found to be typical for all the carbohelicenes. The first stage, characterized by a very high elastic modulus, will be discussed in terms of the van der Waals (vdW) interaction in the section 5.3.

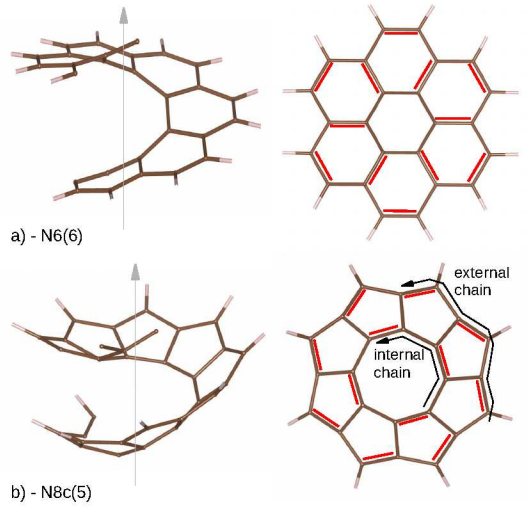

Fig. 4 Supposed bonding configuration for hexagonal (represented by N6(6)) and non-hexagonal (represented by N8c(5)) helicene.

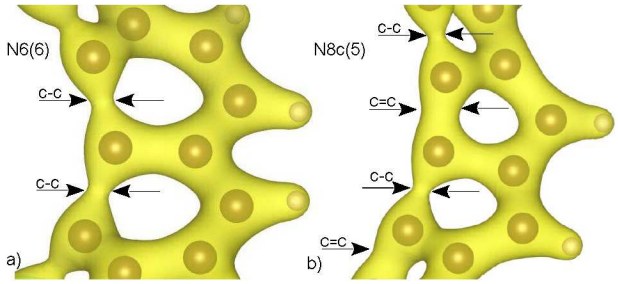

Fig. 5 The detail of the charge-density isosurface close to the maximum reversible strain ε_M for (a) hexagonal helicene N6(6) and (b) non-hexagonal helicene N8c(5). The arrows indicate the necking of the charge-density isosurfaces related to the weak bonds located at the internal atomic chain of the helicene spring with marked C-C and C=C bonds.

5.2 Bonding configurations

The carbon is a tetravalent atom and thus, in graphene sheet, each atom contains two single (C-C) bonds and one double bond (C=C). Consequently, the same bonding was considered in the helicene N6(6) which configuration is depicted in Fig. 4a. In general, all helicenes containing only hexagonal rings will preserve such a configuration. However, there is a question how hexagonal rings replaced by pentagons or heptagons change bonding across the helicene structure. After a detailed structure analysis where the conditions of comprehensive simple bonds between C-H and only one C=C bond per carbon atom were followed, we assumed a possible configuration for non-hexagonal helicene N8c(5) depicted in Fig. 4b. This configuration consists of alternating C-C=C-C=C bonds at both the internal and the external helicene chain which is also supposed to be present in other non-hexagonal helicenes. To validate this bonding hypothesis we used the charge density isosurfaces to visualize the charge between carbon atoms at the internal helicene chain. The charge density is computed for a helicene configuration strained close to ε_M. Although this charge density is not able to visualize exact positions of π-bonds, it is able to localize the weak bonds. As can be seen in Fig. 5a, the helicene N6(6) contains only C-C bonds inside the internal helicene chain. Indeed, the charge density is equally reduced in all bonds and, consequently, the C=C bonds are located as displayed in Fig. 4a. On the other hand, alternating C-C=C-C=C bonds were found at internal chains of all the helicenes N8c(5) where the hexagonal rings were replaced by pentagons (see Fig. 5b). These findings revealed that replacing hexagons by pentagons or heptagons will change the double C=C bonds positions. The bonding configurations across the internal helicene chain are summarized in Tab. 1 for all studied helicenes. The results also revealed the bonding configuration for helicenes consisting of two different rings in the helicene spiral. If the helicene was constructed by an alternation of hexagons and pentagons, the C=C bonds were located in the hexagonal rings (the pentagon ring failed during the straining) while, for the combination of pentagonal and heptagonal rings, the C=C bonds were found in pentagons (the heptagons failed).

5.3 Fracture mechanism and van der Waals interactions

The fracture behavior was evaluated by a visualization of structures after each deformation step. It was found that two main deformation and fracture mechanisms are present: the first (more simple) one is common for conical and standard shapes and the second one for the stair-like ones. The first mechanism is related to the fact that, close before reaching ε_M, the charge density between carbon atoms with C-C bonds located at the internal chain starts to quickly decrease (see Fig. 5). Once the weakest of the C-C bonds breaks (opens), the stronger ones rapidly recover (closes). Such a small crack created in the structure is associated with a remarkable drop in the total energy in the Fig. 2b. The second fracture mechanism is more complex than the first one and depends on the structure configuration (type of the stair-like carbohelicene). In general, this fracture mechanism causes a local re-configuration of the structure. One of the graphene rings forms an irreversible 3D ledge perpendicular to the adjacent rings. Formation of the 3D ledge also corresponds to the first energy drop as shown in Fig. 2b. This second (local 3D) mechanism is obviously more severe than the first one that allows much higher maximum reversible strain ε_M - see Tab. 1. Fig. 6 contains all three typical shapes of studied carbohelicenes: standard, conical and stair-like shape.

A similarly high stiffness as found in the first deforma-

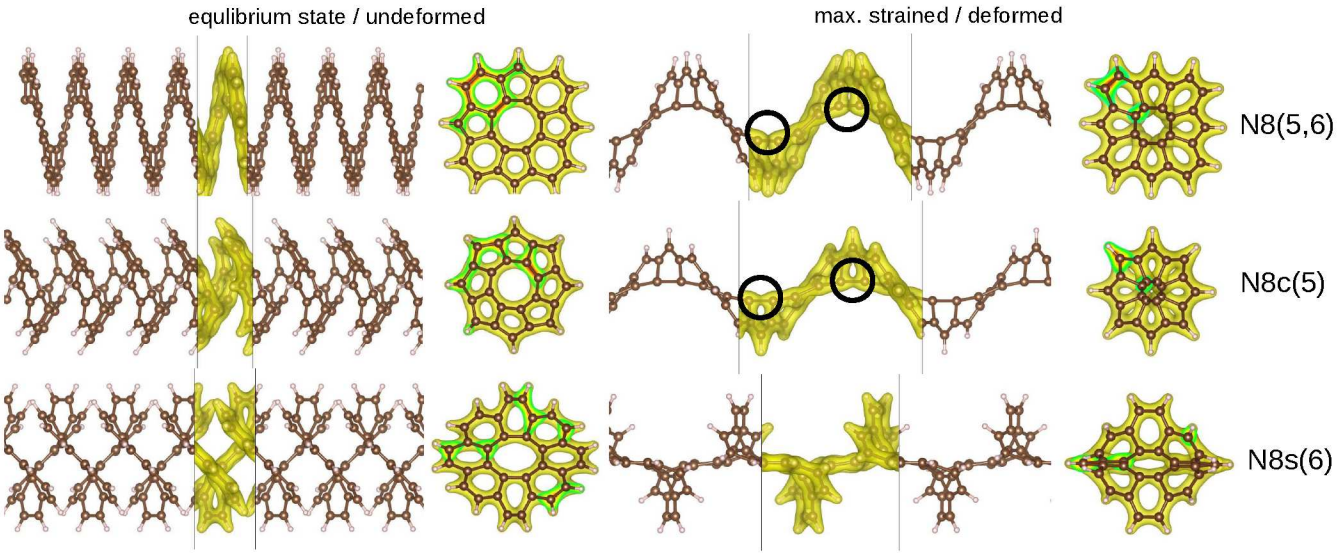

Fig. 6 Three typical shapes of carbohelicenes corresponding to stress-free (equilibrium) and maximum strained states. The top structure represents the standard shape, the structure in the middle is of a conical shape and the bottom structure is of a stair-like shape. The equilibrium/undeformed states of all structures are depicted on the left-hand site and the states close before the first local fracture at ε_M on the right-hand site. The critically deformed structures N8(5,6)and N8c(5) contain weaken bonds (inside the black circles) while a cluster of re-arranged atoms appears in the N8s(6)structure. The green color represents charge density isosurface while yellow color its intersection across the structure.

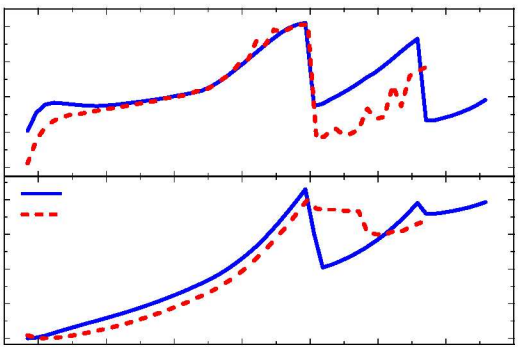

Fig. 7 The tensile test of the N8c(5) carbohelicene with and without DFT-D2 interaction. The change in total energy ΔE_{tot} and the force F are depicted as functions of carbohelicenes elongation in terms of the spiral distance R_p.

tion stage of carbohelicenes was also identified in the tightly wound CNT nanosprings which was attributed to the vdW interaction between atoms of the neighboring turns[24,25]. Moreover, both carbohelical and CNT springs exhibit comparable forces related to initial fracture in spite of the fact that they are formed in a very different way. Because the spiral distance is similar to the distance of graphite sheets a question arised if and how the vdW interactions affect the bond strength during the deformation. Therefore, we performed the DFT simulations both with and without the vdW interactions (DFT-D2[23]). These results are plotted in Fig. 7. As could be expected, the vdW forces play an important role only close to the unstrained state where the spacing between molecular spirals approximately corresponds to the value of 3.35 Å, i.e., to the interfacial distance of graphite sheets. Thus, the inclusion of vdW forces increases the elastic moduli in the beginning of the tensile test but it has no influence on the values of maximal force.

6 Conclusion

The deformation and loading capacity of nine carbohelicenes with different atomic structures were investigated using DFT-D2 calculations. It was found that the presence of defects in the carbohelicene spiral (penta, hepta, etc, instead of hexagonal rings) had a significant influence on their mechanical properties and some carbohelicenes could achieve very large reversible tensile strains (>200 %). Such an extraordinary deformation capacity was typical for standard and conical shapes of the carbohelicenes while those of a stair-like shape exhibited a structure failure even before reaching the strain of 100 %. The latter springs also exhibited the lowest loading capacity. The deformation capacity of the perfect carbohe-

licene N6(6) was the lowest one among the conical and standard springs but it had the highest loading capacity. The roughly assessed effective tensile strength $\sigma_{eff,u} = 117$ GPa of the N6(6) spring is comparable to both the tensile strength $\sigma_{u,t} = 110$ - 121 GPa of a perfect graphene computed using ab initio methods and the strength $\sigma_{u,exp} = 130 \pm 10$ GPa measured by nanoindenation. The bonding analysis discovered that the hexagonal helicenes had only the single C-C-C bonding across the internal chain atoms (most strained bonds) while the non-hexagonal helicenes had the C-C=C bonding at the internal chain. The simulations also revealed that the van der Waals interactions could not be neglected particularly at the earliest stage of deformation but they had practically no impact on either the values of maximal force per bond or those of the maximum reversible strain. The examination of the structure configurations close before reaching the maximum reversible strain revealed the presence of two fracture mechanisms different for stair-like and other carbohelicenes shapes.

Acknowledgments

P.Š. acknowledges the financial support by the project CZ.1.07/2.3.00/30.0005 of Brno University of Technology, J.P. acknowledges the financial support by European Regional Development Fund (CEITEC CZ.1.05/1.1.00/02.0068). The computational resources are provided by the project of NOTUR - The Norwegian Metacenter for Computational Science (www.notur.no).

References

1 M. S. Newman, W. B. Lutz and D. Lednicer, *J. Am. Chem. Soc.*, 1955, **77**, 3420–3421.
2 T. Caronna, M. Catellani, S. Luzzati, L. Malpezzi, S. V. Meille, A. Mele, C. Richter and R. Sinisi, *Chem. Mater.*, 2001, **13**, 3906–3914.
3 R. H. Martin, *Angew. Chem. Int. Ed. Engl.*, 1974, **13**, 649–660.
4 O. Katzenelson, J. Edelstein and D. Avnir, *Tetrahedron: Asymmetry*, 2000, **11**, 2695 – 2704.
5 L. Rulíšek, O. Exner, L. Cwiklik, P. Jungwirth, I. Starý, L. Pospíšil and Z. Havlas, *J. Phys. Chem. C*, 2007, **111**, 14948–14955.
6 Y.-H. Tian, G. Park and M. Kertesz, *Chem. Mater.*, 2008, **20**, 3266–3277.
7 W. Laarhoven and W. Prinsen, *Stereochemistry*, Springer Berlin Heidelberg, 1984, vol. 125, pp. 63–130.
8 D. Beljonne, Z. Shuai, J. L. Brdas, M. Kauranen, T. Verbiest and A. Persoons, *J. Chem. Phys.*, 1998, **108**, 1301–1304.
9 Z. Asfari and J. Vicens, *J. Inclusion Phenom. Macrocyclic Chem.*, 2000, **36**, 101–115.
10 M. Gingras, *Chem. Soc. Rev.*, 2013, **42**, 1051–1095.
11 Y. Shen and C.-F. Chen, *Chem. Rev.*, 2012, **112**, 1463–1535.
12 K. Tanaka, H. Osuga and Y. Kitahara, *J. Org. Chem.*, 2002, **67**, 1795–1801.
13 M. Zhang, K. Zhu and F. Huang, in *Molecular Devices: Molecular Machinery*, John Wiley & Sons, Ltd, 2012.
14 P. Rempala and B. T. King, *J. Chem. Theory Comput.*, 2006, **2**, 1112–1118.
15 T. R. Kelly, J. P. Sestelo and I. Tellitu, *J. Org. Chem.*, 1998, **63**, 3655–3665.
16 C.-T. Chen and Y.-C. Chou, *J. Am. Chem. Soc.*, 2000, **122**, 7662–7672.
17 M. Jalaie, S. Weatherhead, K. B. Lipkowitz and D. Robertson, *Electron J. Theor. Ch.*, 1997, **2**, 268–272.
18 G. Kresse and J. Hafner, *Phys. Rev. B*, 1993, **47**, 558–561.
19 G. Kresse and J. Furthmüller, *Comput. Mat. Sci.*, 1996, **6**, 15 – 50.
20 G. Kresse and J. Furthmüller, *Phys. Rev. B*, 1996, **54**, 11169–11186.
21 G. Kresse and D. Joubert, *Phys. Rev. B*, 1999, **59**, 1758–1775.
22 J. P. Perdew, K. Burke and M. Ernzerhof, *Phys. Rev. Lett.*, 1996, **77**, 3865–3868.
23 S. Grimme, *J. Comput. Chem.*, 2006, **27**, 1787–1799.
24 J. Wu, J. He, G. M. Odegard, S. Nagao, Q. Zheng and Z. Zhang, *J. Am. Chem. Soc.*, 2013, **135**, 13775–13785.
25 J. Wu, S. Nagao, J. He and Z. Zhang, *Small*, 2013, **9**, 3561–3566.
26 F. Liu, P. Ming and J. Li, *Phys. Rev. B*, 2007, **76**, 064120.
27 C. Lee, X. Wei, J. W. Kysar and J. Hone, *Science*, 2008, **321**, 385–388.